Peer-Reviewed Technical Communication

Visual and Passive Acoustic Marine Mammal Observations and High-Frequency Seismic Source Characteristics Recorded During a Seismic Survey

John R. Potter, *Senior Member, IEEE*, Marielle Thillet, Craig Douglas, Mandar A. Chitre, *Member, IEEE*, Zbigniew Doborzynski, and Paul J. Seekings

***Abstract*—In this paper, we present marine mammal observation statistics, high-frequency seismic source characteristics, and example denoising of marine mammal acoustical recordings using data collected during the mitigation and monitoring program for a 3-D seismic survey by EnCana Corporation, Calgary, AB, Canada, in the Northwest Atlantic during 2003. Marine mammals were observed both visually and acoustically. No marine mammal incidents or adverse reactions were observed during the survey. Acoustical observations were made by the Seamap Passive Acoustic Cetacean Monitoring System (SPACMS), consisting of two hydrophones placed 50 m apart, towed ahead of and to one side of the seismic source. Visual and acoustical detections were uncorrelated, indicating the complementary nature of the two observational techniques. Visual detections were more common per hour of effort than acoustical detections. Acoustical detection rates showed no significant day–night difference. Marine mammals appeared to have avoided very close ranges (<100 m) from the seismic array during seismic acquisition, but the overall number of marine mammals in the observable radius (1–2 km) did not change significantly when the seismic source was "on" compared to "off." Marine mammals were observed in larger groups and appeared to have become less vocal when the seismic source was active. It should be noted however, that the results from this data gathering effort may be affected by potential sources of bias (such as the combination of data from toothed and baleen whales). Signal processing of seismic source signatures indicated some high-frequency energy content consistent with expectations from earlier work. This analysis confirmed that most of the seismic energy was concentrated at lower frequencies (<500 Hz). No low-frequency comparisons with near-field data could be made due to the geometry of the SPACMS recording hydrophones and seismic source, which resulted in the Lloyd's mirror effect obliterating low-frequency components in the SPACMS records. A wavelet-based denoising method was applied to improve the visibility of marine mammal vocalizations on a spectrogram display.**

***Index Terms*—Acoustics, beaked whale, marine mammal, seismic surveying.**

Manuscript received March 10, 2005; revised November 1, 2005; accepted November 29, 2005.

Associate Editor: J. F. Lynch.

J. R. Potter, M. A. Chitre, and P. J. Seekings are with the Acoustic Research Laboratory, Tropical Marine Science Institute, National University of Singapore, Singapore 119223, Singapore (e-mail: johnpotter@arl.nus.edu.sg).

M. Thillet and Z. Doborzynski are with EnCana Corporation, Calgary, AB T2P 2S5, Canada.

C. Douglas was with Seamap Pte. Ltd., Singapore 508913, Singapore. He is now in independent Oil Exploration Industry Consultant.

Digital Object Identifier 10.1109/JOE.2006.880427

I. Introduction

ENCANA CORPORATION contracted WesternGeco's M/V Triton to acquire a 1734 km^2 3-D seismic survey in May–June, 2003, over its Stonehouse exploration license (EL 2414), offshore Nova Scotia, Canada. The survey area is located over the Scotian slope in water depths of 300–2500 m [see Fig. 1(a) and (b)]. The western boundary of the survey area is adjacent to Haldimand canyon, which is an occasional habitat for the northern bottlenose whale (*Hyperoodon ampullatus*), a population of beaked whales designated as "endangered" in December, 2002 [1]. Their primary habitat is the Gully Marine Protected Area, and they are also found in Shortland canyon, located 70 and 47 km west from the survey area, respectively. Timing of mating, calving, as well as presence in Haldimand canyon is unknown. The preferred habitat of northern bottlenose whales is centered on the 1000-m depth contour, and they are rarely sighted in water depths of less than 800 m. Nova Scotia is the southern limit of this species, and the Scotian Shelf population appears to be isolated from its nearest neighbor population in the Davis Strait, off northern Labrador, 1400 km to the north.

During environmental assessment consultations, specific concerns were brought up about the potential impact of the survey on the northern bottlenose whale due to its proximity to Haldimand canyon, and suspected enhanced susceptibility of beaked whales to acoustical impact [2]. An operational plan to protect and monitor marine mammals in the survey area was drawn up for the survey, including a safety-zone monitoring program using both visual and passive acoustic monitoring with the Seamap Passive Acoustic Cetacean Monitoring System (SPACMS). An approach of responsible risk management was followed to select a radius that would likely provide reasonable protection at realistic ranges. A shutdown safety range of 800 m was selected for "endangered" whale species, which include the northern bottlenose whale, North Atlantic right whale, and blue whale. None of those species were observed within the 800-m range during seismic activity, so no shutdown was ever initiated for marine mammals.

Subsequently, EnCana decided to analyze the data collected during the monitoring program and conduct research. Since the program was not designed for research purposes, systematic

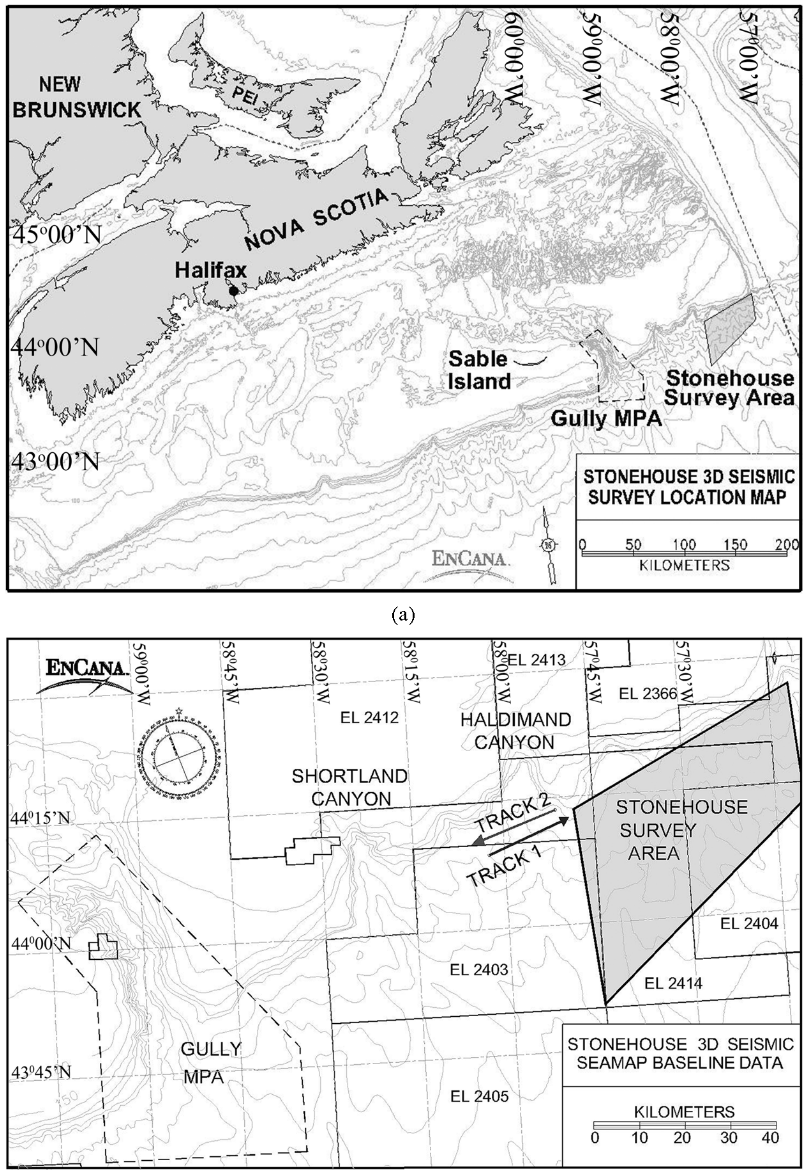

(a)

(b)

Fig. 1. (a) Stonehouse 3-D seismic survey location map. (b) Detail of seismic survey area, showing nearby canyons.

presurvey and postsurvey marine mammal abundances were not taken. However, two SPACMS survey lines were acquired within Haldimand canyon before seismic operations started, and no northern bottlenose whales (nor any other whale species) were detected [see "Track 1" and "Track 2" on Fig. 1(b)]. Visual and acoustical observational schedules also differed significantly, the SPACMS system being decommissioned earlier in the survey when the seismic vessel drew further away from the region of highest perceived risk to the northern bottlenose whale.

Marine mammal observer (MMO) duties were conducted primarily by EnCana's marine mammal, bird, and fishery liaison observer and by crewmen with binoculars during daylight hours and when visibility permitted. These duties were also conducted by bridge officers. All received training from the Department of Fisheries and Oceans (DFO) before the survey. A continuous watch was maintained on the bridge. Each sighting was logged on a marine mammal recording form and included in the daily report. Information was also passed to the SPACMS operators for cross reference and inclusion into a detection summary report; any acoustical detection was visually confirmed whenever possible.

There were no other seismic vessels operating in the immediate area of the survey. However, slight seismic interference was observed on one line, possible due to the Geophysical Service Incorporated Admiral (GSI Admiral), a seismic vessel known to be operating on the Scotian Shelf at the same time. Shipping activity in the survey area was negligible, and fishing effort was low.

This paper presents the configuration of the SPACMS (Section II), the geographical distribution of observed marine mammals (Section III), a statistical analysis of marine mammal observations (Section IV), a high-frequency seismic source analysis (Section V), and a technique for marine mammal vocalization denoising with examples from this data set (Section VI).

II. Configuration of the SPACMS

SPACMS was used to complement the standard visual observations conducted during daylight hours to extend the capability to detect marine mammals. One senior Seamap operator and two trained crewmen operated the SPACMS. The benefits of a passive acoustic observation system include the following:

- detects 24 h a day, whereas visual monitoring is not effective during periods of low visibility (night, fog, or rain);
- works reasonably well even in poor weather arising from high winds, when visual observations become difficult;
- provides a complementary detection method unrelated to how long a particular species involved in a particular behavior is at the surface to be seen.

The disadvantages compared to visual observations include the following:

- equipment is more expensive;
- requires heavier equipment and longer deployment/recovery times;
- may interfere with in-sea seismic equipment;
- does not detect nonvocalizing marine mammals;
- difficult to get accurate ranges on faint contacts and, to a lesser degree, bearing.

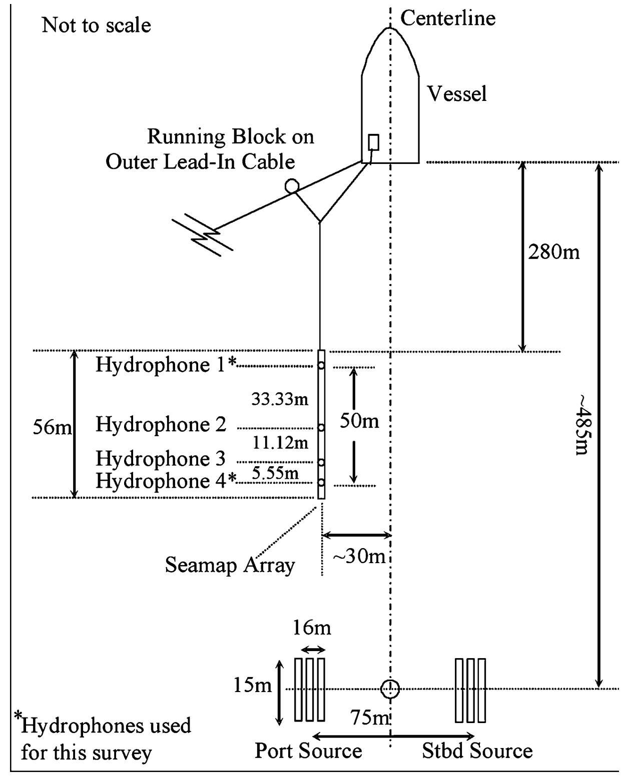

Fig. 2. Vessel layback diagram, showing deployment position of the SPACMS.

A. Sensor Description and Deployment

SPACMS consists of a towed hydrophone array with four hydrophones at various separations from 5.55 to 50 m of which two can be monitored at one time. Because of the specific interest in blue whales which vocalize at low frequencies, it was decided to monitor the two most spatially separated hydrophones (50 m) to give the maximum amount of phase difference in the arriving low-frequency signals. The hydrophones have a sensitivity of -201 dBV re 1 μPa and are sampled at a rate of 44 kHz. The hydrophones are spectrally flat to within $+/-1.5$ dB over 1 Hz–15 kHz. A fixed gain preamplifier in the streamer provides 27 dB of gain. The dual channel 50-m array was deployed 280 m behind the vessel, ahead and slightly to the port side of the seismic source (which was towed $\sim$485 m behind the vessel) to ensure that it did not interfere with the recovery and deployment of the in-sea seismic equipment (see Fig. 2).

B. Signal Displays

The acoustical signals received by the streamer were fed to the interface unit; then to the computer for processing, recording, and display. The displays showed the operators the detected clicks, ultralow-frequency signals and wideband spectrogram information on spectrogram plots. Streamer depth and position were also displayed. The signals from the hydrophones were also processed to obtain a bearing to the operator-selected acoustical source using the measured time of arrival delay from one hydrophone to the other and a simple direct ray assumption. Using global positioning system (GPS) positioning information and a proprietary mapping application, an approximate range for an acoustical source can be estimated based on a "running fix" obtained by recording a series of bearings over time, forming an incoherent synthetic aperture.

Unfortunately, towing the entire seismic spread and using azimuth thrusters produced high levels of mechanical and cavitation noise. This had not been observed during the test deployment in the Gulf of Mexico, where the full streamer array and position control systems were not deployed. This broadband noise reduced the maximum detection ranges for vocalizations from the theoretical detection range of several kilometers (depending on species) to approximately 1–2 km; however, this was still adequate for mitigation purposes.

Acoustical monitoring for whales over the frequency range 0–22 kHz was conducted almost continuously over the 22-d deployment period during seismic activity with a duty cycle of approximately 75%. Operators monitored for whales before and during the ramp-up period and while the vessel was in production.

III. Geographical Distribution of Marine Mammal Sightings

A chart of the marine mammal sightings is shown in Fig. 3. Marine mammal species are represented by different symbols. If no specific bearing or distance was available for the marine mammal sighting, the vessel position is indicated instead of the marine mammal position. Visual sightings are prefixed with the letter "V" whereas SPACMS acoustical sightings are prefixed with the letter "S." A total of eight visual sightings are not plotted, being south of the chart coverage.

Most of the sightings were along the northern edge of the survey area, while the vessel was turning at the end of a seismic

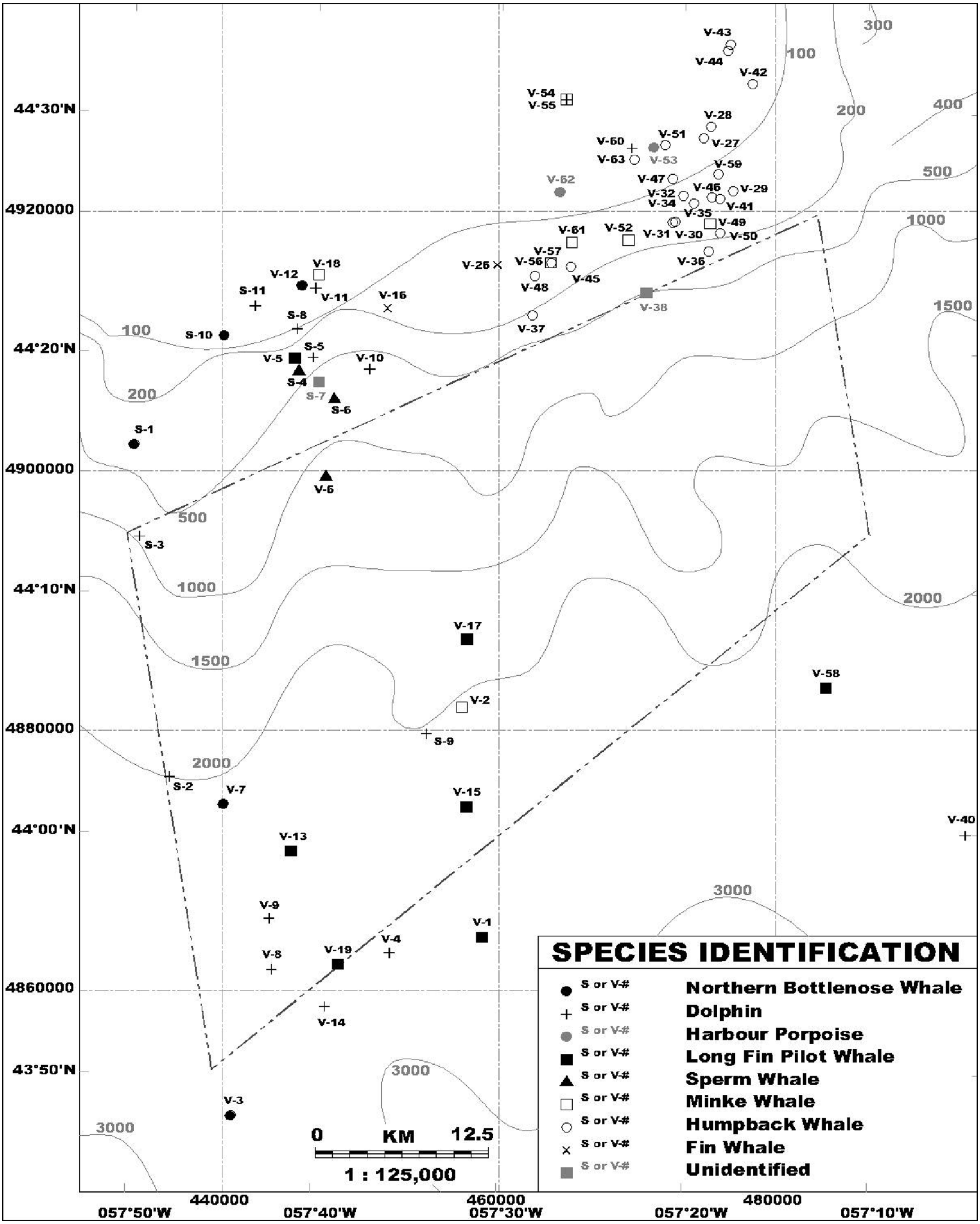

Fig. 3. Chart of marine mammal detections during the Stonehouse survey.

line and aligning itself for the next. This suggests that marine mammals are more attracted to the vessel while the seismic source is turned "off" (for approximately 3 h per turn). It could also be that marine mammals congregate in shallower waters

TABLE I
DETECTION EVENTS DURING THE SURVEY FOR THE VISUAL AND ACOUSTICAL OBSERVATIONS

	BW	D	HP	PW	SW	MW	HW	FW	UI	Total
Acoustic	2	11	0	0	3	0	0	0	1	17
Visual	3	14	2	7	2	7	25	3	1	64
Total	5	25	2	7	5	7	25	3	1	81

BW=Northern Bottlenose whale; D=Dolphin; HP=Harbour porpoise; PW=Long Fin Pilot whale; SW=Sperm whale; MW=Minke whale; HW=Humpback whale; FW=Fin whale; UI=Unidentified

of the Scotian slope (<500 m deep or so). The Scotian Shelf edge is indeed a whale migration route, especially in the spring and early summer as whales come back from their south winter grounds, with later entry onto the Shelf.

IV. STATISTICAL ANALYSIS OF MARINE MAMMAL SIGHTINGS

Acquisition of the Stonehouse survey started on the west side of the survey area, near Haldimand canyon, and moved eastwards over the period May 3–June 28 (57 d). SPACMS was operated continuously during seismic acquisition from May 3–24 (22 d), after which the seismic vessel drew further away from the region of highest perceived risk to the northern bottlenose whale. Visual observations started three days before commencement of seismic activity (April 30) and continued until the end of the program on June 28 (60 d in total). Much of the daytime weather during this period was foggy, with significant waveheights varying from <1 m to >5 m.

There are several differences in the type of information gathered from the visual and SPACMS observations. Visual detections can estimate the number of animals; SPACMS cannot. To be able to compare data obtained from the two methods, we have therefore used the number of "detection events" rather than number of animals. An acoustical detection event is defined as the detection of one or more marine mammals; acoustical detections too faint to derive a range were disregarded. We have also normalized detection rates by hours of observation effort to compare SPACMS (which can operate 24 h a day) and visual observations (which can operate only 14 h or less per day, depending on weather).

We begin by looking at the number of detection events, split into visual and acoustical detections and not normalized by hours of effort. Ideally, we would have liked to take the visual observations only for the period where SPACMS was operating, for a direct comparison, but the period (May 3–24) was too short to obtain statistically significant number of visual events; and so visual detection events have been considered from the entire survey. This introduces some geographical/temporal confounding variables, as we will see. Table I shows the number of detection events for the two methods, with the key shown below the table contents.

Of the 17 acoustical detection events, 11 were in daylight, in line with the proportion of daylight hours at this latitude in May. Hence, acoustical detection rates are similar for day and night. This supports the assumption that we may compare hourly detection rates between visual and acoustical techniques irrespective of the concern that acoustical monitoring operates during daytime and night time, whereas visual monitoring is limited to daytime.

Of the 11 daylight acoustical detections, eight were dolphin whistles and three sperm whale echolocation click trains—one of which occurred twenty minutes after the last visual observation of sperm whales. Of the six detections at night, three were dolphin whistles, two were identified as northern bottlenose whales echolocation clicks, and one was click trains too weak to identify.

There were no acoustical detections of mysticetes, although we know from previous programs that SPACMS can detect baleen whales species. Humpback whales were visually observed during the latter part of the survey, when SPACMS was not operating. This is, therefore, likely to be a temporal bias. For minke and fin whales, it may be that these species were not vocalizing, or that their low-frequency vocalizations are more easily lost in the background vessel noise; whereas transient, high-frequency echolocation clicks from toothed whales are quite distinct and more easily detected. This is borne out by the relatively high detection rate (compared to visual detections) for sperm whales, northern bottlenose whales, and dolphins, compared to other species.

The detection of northern bottlenose whales was of particular importance. There were five such detection events, three visual, and two acoustical. Acoustical detections of northern bottlenose whales were identified by SPACMS operators based on the observed vocalization pattern. All events occurred during weather standby or line turns, while the seismic source was not active. The closest detection was at 30 m during weather standby. Other detections were at ranges of 500–1800 m.

Noting that no detection event of any species was recorded both visually and acoustically, and that two out of five of the northern bottlenose whale detection events were acoustical, indicates the complementarity of visual and acoustical monitoring. Some contributing factors to the lack of correlation between visual and acoustical detections are temporal bias (e.g., humpback whales), periods of low visibility when visual detections are limited (fog, night), and diving/vocalizing behavior of the whales (e.g., some whale species tend to be silent when they are at the surface, and to vocalize when they are involved in underwater activities such as chasing squids).

A. *Marine Mammal Response to Seismic Activity*

At no time was any individual observed to be affected by seismic activity. However, statistical analysis of marine mammal detections can draw out more subtle effects such as minor avoidance.

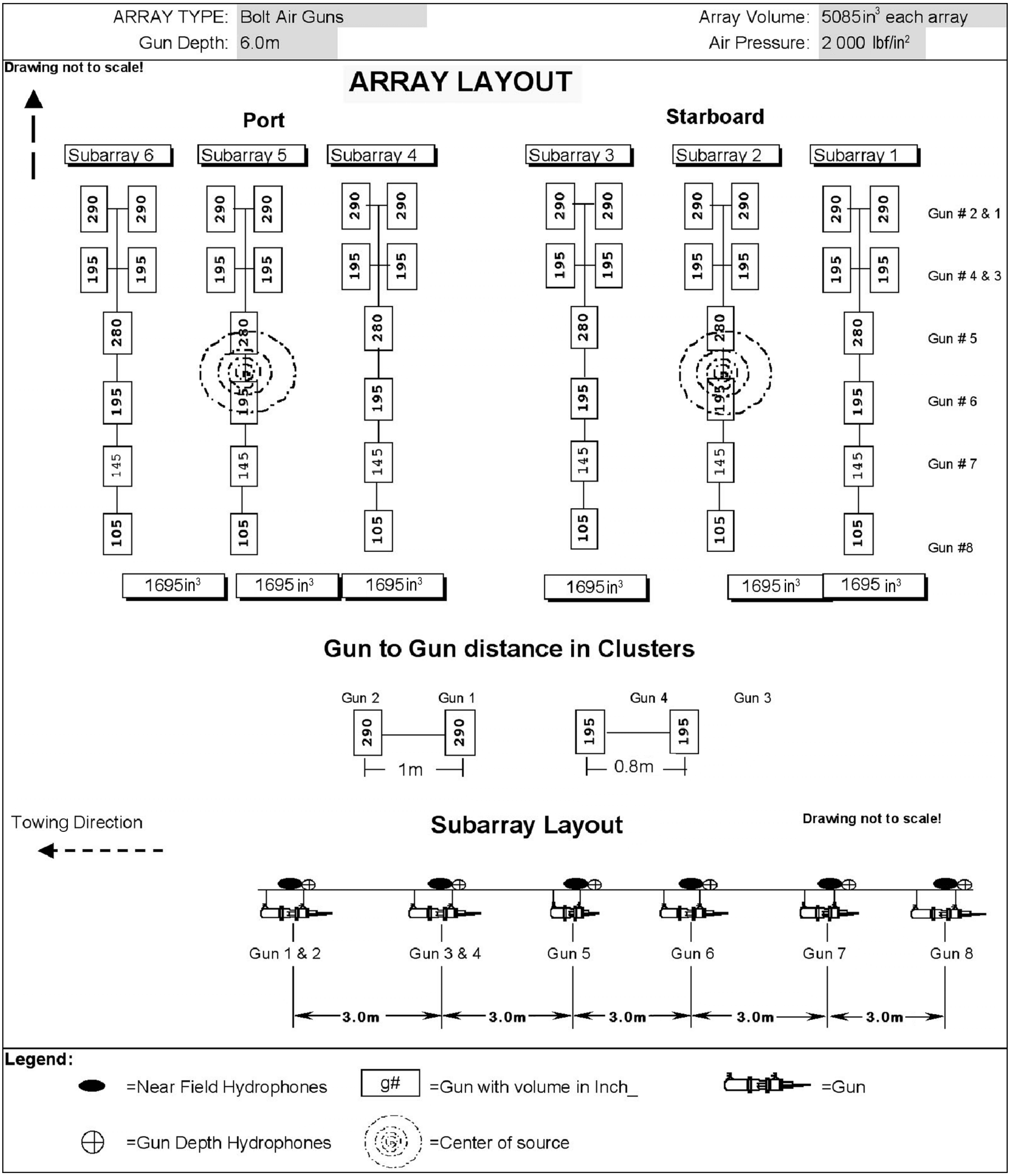

Fig. 4. Layout of the Stonehouse seismic source.

Statistics were computed taking time bins of 6 min (0.1 h); for reporting purposes, values are stated in detections per hour. Standard T-tests were used to assess statistical significance. Ideally, statistics for toothed whales and baleen whales should have been analyzed separately because of differences in hearing range, but the small number of samples did not allow for this, potentially introducing bias. Other potential sources for bias include location/water depth differences, different observers and differences in detection ranges. As expected for a program not initially planned for research, the experimental design is

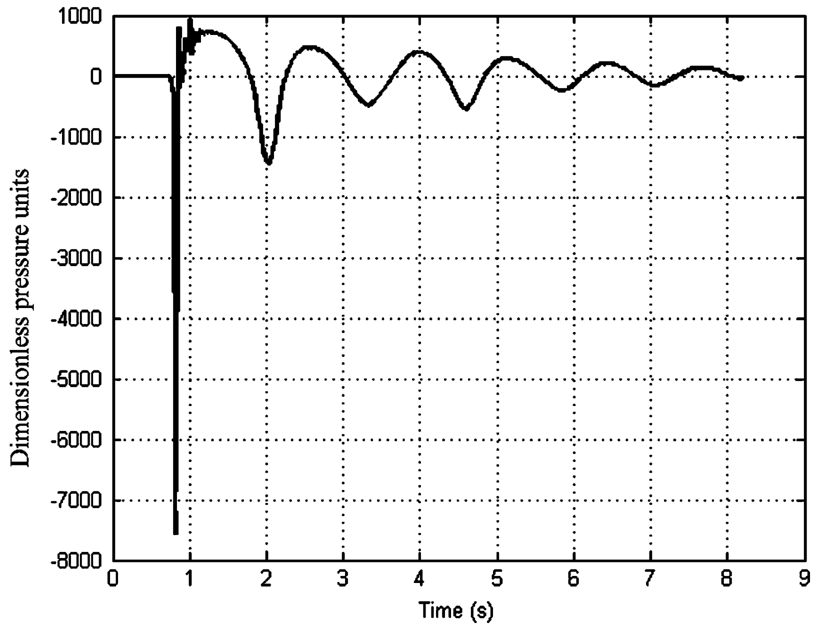

Fig. 5. Example trace (with arbitrary vertical pressure scale) from the near-field recordings.

not well blocked (in terms of optimally sampling the parameter space to unravel confounding variables) and some of these sources of errors are likely to cause some bias.

B. Visual Detection Versus Seismic Activity

The number of detection events/hour with seismic source "off" versus "on" gives a ratio of 2.5 : 1 (number of visual detection events per hour of observation with source "off" = 0.089 and source "on" = 0.035). This is statistically significant at the 99.7% level.

This ratio approaches unity (1.16 : 1) if we use animal counts (0.52 for source "off" to 0.45 for source "on"). This is statistically significant only at the 64% level—little better than chance.

The combined implication of these two results is that marine mammals did not as a whole move out of visual range or become less visible when the seismic source was active but congregated in fewer, but larger, groups.

C. Acoustical Detection Versus Seismic Activity

Acoustical detection events/hour versus seismic activity has a ratio of 3.3 : 1 (0.0574 for source "off" to 0.0175 for source "on"). This is a statistically significant difference at the 98.6% level. Coupled with the visual results computed in Section IV-B, this implies that the whales tend to become less vocal but do not go away when the seismic source is active. This could have implications for possible bias inherent in using visual observations to interpret the impact on marine mammals. Seismic surveying can apparently have a behavioral impact at a high level of statistical significance without visual observers reporting seeing fewer marine mammals.

D. Marine Mammal Proximity Versus Seismic Activity

SPACMS was not able to estimate ranges sufficiently often to obtain statistically significant results, owing to the difficulty in maintaining contact over a long enough period for a long baseline bearing change.

The average detection range from visual observations does not show a significant difference between seismic source "off" and "on." However, the percentage of detection events within 100 m does (35% for source "off" versus 14% for source "on"), suggesting that marine mammals do avoid very close ranges when the seismic source is "on" compared to "off," even if they do not move far enough to exceed visual detection range. Safety-zone monitoring did not affect those statistics since no shutdown was required during the survey.

V. Seismic Source Signal Analysis

Acoustical recordings of the seismic source elements were made at low sampling rates (500 and 2000 Hz) by near-field receivers (approximately 1 m from the source elements) and at high sampling rate (44 kHz) by the two SPACMS receivers. The SPACMS data allow the high-frequency content of the seismic signals to be estimated as reported elsewhere, e.g., [3]. The near-field receiver recordings were lowpass filtered at 500 Hz. The far-field SPACMS receivers were at some 35-m depth, and at a range of 147–224 m from the seismic source elements, so that the difference between the direct and surface-reflected arrivals was very short, canceling out frequency components below about 250 Hz. Hence, there is little overlap between the two recording system signal estimates that would allow comparison.

The seismic source used consisted of two identical 5085-in^3 source arrays laterally separated by 75 m, operated in flip-flop mode. Each array consisted of three 1695-in^3 subarrays operating at 2000-lbf/in^2 air pressure (Fig. 4).

Fig. 5 shows example traces from the near-field hydrophones, on an arbitrary pressure scale. It is clear that (apart from the geophysical recording standard inversion of the signal) the near-field signal from a single source element consists of a single rapid pulse rise and subsequent rapid fall, followed by periodic bubble plume pulses at a little over 1-s intervals. Once the surface reflections and array tuning are taken into account, most of

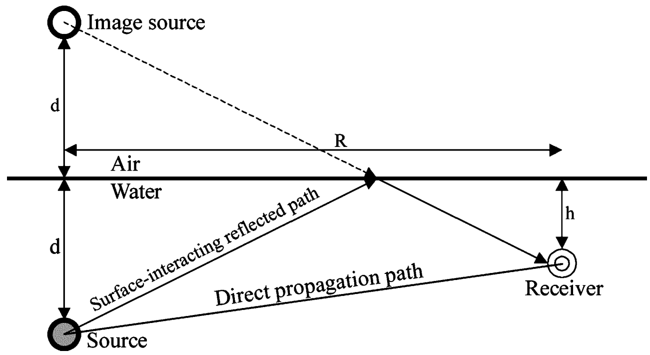

Fig. 6. Geometry for Lloyd's mirror. The range R is normally $\gg h$ or d.

the energy is concentrated around 50 Hz for the seismic array. The smaller sharp inverted peaks visible shortly after the primary pulse are presumed due to surface-reflected signals, much attenuated due to the additional distance traveled by the reflected path compared to the nearness of the near-field hydrophone directly above the source element port. From the ratio of the amplitudes and the delay interval between primary and reflected path, the near-field hydrophone is estimated to be approximately $1.25 +/-0.25$ m from the source element port, consistent with its actual location on the source array (1 m for a single source element position and 1.25 m to the centroid of a cluster).

A. SPACMS Recordings

The SPACMS receivers were at a nominal depth of 35 m with ranges to the various seismic source elements varying between 147–224 m for the two hydrophones (144–222 m for horizontally projected distances). Both source arrays were at a depth of 6 m.

For a sound source near a perfectly compliant boundary, like the boundary between water and air at the sea surface, the boundary can be replaced by an image source with opposite sign (π radians out of phase) placed equidistant on the far side of the boundary. This "image source" causes destructive and constructive coherent interference with the direct source signal, depending on range, depth, and frequency. It is then easy to see that a source near a compliant reflecting boundary is likely to generate a complicated pressure amplitude field. This effect is known as Lloyd's mirror [4]. An example of a typical Lloyd's mirror geometry is given in Fig. 6.

We write the direct path signal p_1, as a spherically decaying Fourier sum

$$p_1 = \sum_i \frac{P_i \cos(w_i t - k_i R_1)}{R_1} \tag{1}$$

where R_1 is the direct distance from source to receiver.

The surface-reflected wave, p_2, appears to arrive from a virtual image source at a different range R_2, and is also negative because of the phase reversal, giving us

$$p_2 = \sum_i \frac{-P_i \cos(w_i t - k_i R_2)}{R_2}. \tag{2}$$

If $R \gg h$, d (valid for our case), we may linearize the expressions for R_1 and R_2 in terms of R, h, and d and combine the two signal terms to give an approximation for the combined signal pressure amplitude in the form

$$p = p_1 + p_2 = \sum_i \frac{-2P_i}{R} \sin\left(\frac{k_i h d}{R}\right) \sin(\omega_i t - k_i R). \tag{3}$$

Equation (3) contains the usual sinusoidal oscillations in space and time for the individual Fourier components, and also has the slowly decaying $1/R$ dependence due to spherical spreading. There is also another sinusoidal term, however, with argument (khd/R) that modulates the root-mean-square (rms) pressure amplitude of each component and, at large range and low frequencies, tends to zero. This is to be expected, since a receiver is exposed to a source and a virtual "antisource" (an image π radians out of phase) with little angular separation ($R \gg d, h$) so that the two sources coherently cancel where the difference in transmission path lengths is small compared to the wavelength.

For our case, $h \sim$35 m and $d \sim$6 m, while $R \sim$144–222 m. Equation (3) predicts that at 250 Hz there will be coherent constructive interference at 144-m range, while the amplitude will be reduced by 45% from 144 to 222 m. At lower frequencies, the signal is progressively reduced at all ranges over 100 m. At 100 Hz, the most distant SPACMS hydrophone receives amplitude reduced by 8 dB.

Therefore, to estimate the free-field[1] seismic source element signal from the SPACMS recordings is not so simple, because the direct and reflected paths are of very similar lengths and the angle of incidence on the surface is extremely shallow, permitting an almost specular return of similar amplitude to the direct path. The method chosen in this analysis is deconvolution of the direct and surface-reflected signals, accepting that frequencies below about 200 Hz will be irretrievable.

B. Deconvolution Algorithm

Let $x(t)$ be the free-field transmitted signal, with the received signal $y(t)$ at each of the two SPACMS hydrophones modelled as the superposition of an undistorted direct path replica and a delayed surface-reflected path replica with 180° phase shift, the time lag between the direct and surface-reflected arrivals being different for the two hydrophones. Let $h_1(t)$ be the impulse response of the channel between the source and hydrophone 1 and $h_2(t)$ be the impulse response of the channel corresponding to hydrophone 2. Ignoring amplitude modulation due to spherical spreading and absorption (which we take to be similar for both paths)

$$\begin{aligned} h_1(t) &= \delta(t) - \delta(t - T_1) \\ h_2(t) &= \delta(t) - \delta(t - T_2) \end{aligned} \tag{4}$$

where T_1 and T_2 are the time lags, so that for the two receiving hydrophones, we have

$$\begin{aligned} y_1(t) &= h_1(t) \otimes x(t) + n_1(t) \\ y_2(t) &= h_2(t) \otimes x(t) + n_2(t) \end{aligned} \tag{5}$$

where $n_1(t)$ and $n_2(t)$ are the noise terms, which in general are assumed to be much smaller than the signal.

[1]Free-field signal refers to the signal that would be received in the absence of reflecting boundaries.

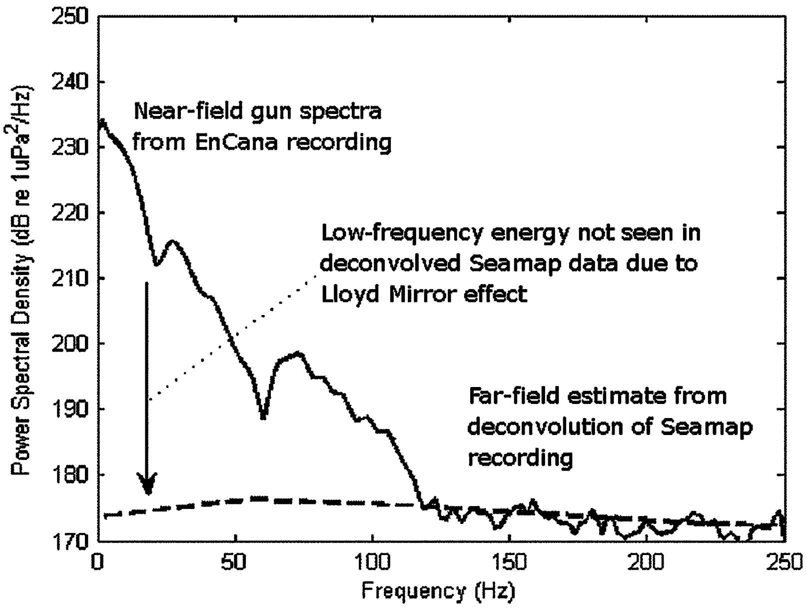

Fig. 7. Comparison of a near-field EnCana and deconvolved SPACMS spectra at low frequencies.

A polynomial division by $h(t)$ allows us to estimate $x(t)$ from $y(t)$ in the absence of noise. However, such a division is sensitive to noise and causes undesirable oscillations in the estimate of $x(t)$.

In general, we do not know the time lags for the hydrophones. We can estimate these by assuming that the correct $h(t)$ will minimize the energy in the estimate of $x(t)$. By performing an exhaustive search over the physically possible time lags (based on the geometry), we choose the time lags for the two hydrophones that minimize the energy in the estimated $x(t)$

$$T_1 = \underset{T}{\operatorname{argmin}}\{\operatorname{deconv}\langle y_1(t), h(T)\rangle\}$$
$$T_2 = \underset{T}{\operatorname{argmin}}\{\operatorname{deconv}\langle y_2(t), h(T)\rangle\} \tag{6}$$

where $\operatorname{deconv}\langle\ldots\rangle$ is the polynomial deconvolution operator and $h(T)$ is the impulse response corresponding to time lag T.

For signals of finite length, the impulse response $h(t)$ can be written in a matrix form

$$y = Hx \tag{7}$$

where y is the column vector containing the convolved signal and x is a column vector containing the original signal. Based on the two time lags T_1 and T_2, we determine $h_1(t)$ and $h_2(t)$ and consequently the matrices H_1 and H_2. As both hydrophones receive the same source signal convolved with different impulse responses, we can write

$$\begin{pmatrix} y_1 \\ y_2 \end{pmatrix} = H_T x$$
$$H_T = \begin{bmatrix} H_1 \\ H_2 \end{bmatrix}. \tag{8}$$

The matrix H_T is in general not a square matrix and does not possess an inverse. However, a generalized pseudoinverse ${H_T}^+$ can be computed using the singular value decomposition (SVD) of H_T. The pseudoinverse finds a least mean-square (LMS) error solution for the system and, therefore, is robust to small noise terms

$$H_T = USV^T$$
$$H_T^+ = VS^{-1}U^T. \tag{9}$$

Hence, the estimate $\hat{x}(t)$ of $x(t)$ is given by

$$\hat{x} = H_T^+ \begin{pmatrix} y_1 \\ y_2 \end{pmatrix}. \tag{10}$$

This simultaneous use of both received signals in a least-squares optimization sense is chosen for its robust performance in the presence of noise. However, the estimate seems to still contain some high-frequency oscillations. Assuming that the original signal is spectrally smooth, we can impose an additional constraint of spectral smoothness on $\hat{x}(t)$ by smoothing the fast Fourier transform (FFT) of $\hat{x}(t)$ using the locally weighted linear regression (LOWESS) algorithm [5]. This algorithm removes outliers, resulting in a smooth spectrum. A smoothing length of 20 samples was arbitrarily chosen by visual inspection of the results. A comparison between the low-frequency energy density recorded by a near-field hydrophone from the source array and the energy density estimated by the deconvolution of the SPACMS recording is shown in Fig. 7, with absolute levels adjusted to match at crossover since the calibration of the pressure signal from the near-field hydrophones is not known. The dashed line is that obtained for deconvolution, whereas the solid line shows the low-frequency near-field hydrophone results.

As expected, the deconvolved result falls progressively below the near-field result for low frequencies, with a shortfall of some 10 dB at 100 Hz, broadly in line with estimates made from (3) for the Lloyd's mirror effect. The higher energy levels below 100 Hz shown in the near-field curve would not be experienced in a seismic source array, where tuning removes almost all energy below 50 Hz.

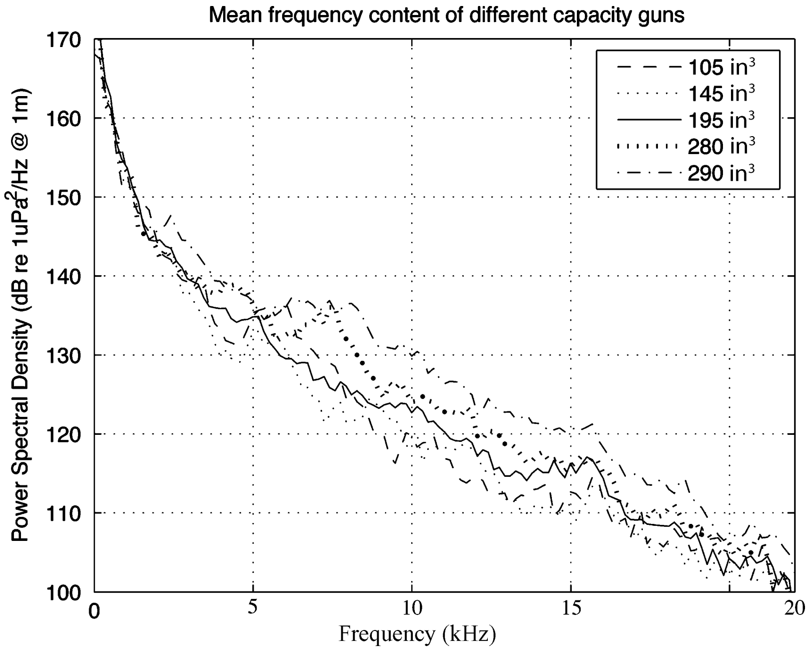

Fig. 8. High-frequency power spectral density for airguns of various sizes.

We can, therefore, proceed to examine the high-frequency properties of the source element signals estimated by deconvolution, bearing in mind that the time-series representation will not be useful (since most of the energy in the signal is lost at low frequencies) and that frequency components should only be trusted above about 200 Hz. Although most seismic energy is concentrated at low frequencies and emitted at a steep launching angle (downward to bottom), high-frequency analysis is useful because some high-frequency energy is still generated and propagates outward, especially in a mixed surface layer. Surface ducting tends to amplify the high-frequency sound emitted by seismic surveys, as was observed in the Gulf of Mexico sperm whale seismic study conducted by the U.S. Minerals Management Service. Its potential for impact may, therefore, be higher than at first can be expected from a seismic source.

C. Deconvolved High-Frequency Results

We present examples of high-frequency spectral power density for seismic source elements of various sizes in Fig. 8. The curves are averages over all source elements of each size for which recordings are available. The general trend is clearly for all sizes to exhibit decreasing power as frequency increases, with levels at 5 kHz some 65 dB below those at 50 Hz estimated from Fig. 7. As expected, larger source elements produce generally higher energy levels at all frequencies. There is no indication of marked frequency structure in any of the sizes, or any significant difference in spectral shapes, indicating that these source elements all operate in much the same way, simply with larger or smaller gas releases as the size suggests.

Examination of different signatures from each source element shows that the source elements are very stable in their output. An example of four signatures from source element 2–3 (element 3 from subarray 2; 195 in^3) is shown in Fig. 9.

When a source element signature is combined with its reflection in the surface, the spectral density could be as much as 6 dB higher (for coherent constructive interference) or reduced to zero. A simulation of the effect of elevation of a receiver at 100 m has been carried out to indicate how received levels might be affected by the depth of a receiver at constant range. The results have been corrected for spherical spreading to give the apparent source level at 1 m. The results for source element 2–3 are shown in Fig. 10. As can be seen, the energy density at steep angles (high declination from the horizontal) at low frequencies is somewhat higher than for the signature shown in Fig. 9 for this source element. At frequencies below 4 kHz, there is a significant reduction in received level if the receiver is nearly horizontal, with little or no effect below a declination of 30°. At higher frequencies, there is no apparent declination effect.

Whereas it is often assumed that the array will always steer seismic energy downwards (which is certainly true at low frequencies), we see here that this is not as obvious at higher frequencies, where many odontocetes hear best (though the amplitude of these higher frequency signals is attenuated very rapidly to ambient noise levels).

Finally, the effect of an entire source array was simulated, with surface reflections. The power spectral densities above 150 Hz were estimated at declinations of 0°, 30°, 60°, and 90°, 90° being directly downward from the surface. The array is not rotationally symmetric and, hence, exhibits azimuthal variation. For a declination of 90° (pointing straight down), there is no azimuthal variation. For other angles of declination (0°, 30°, and 60°), spectra were computed in five azimuthal directions, 0°, 45°, 90°, 135°, and 180°, where 0° is ahead and 90° is broadside of the array. The results are shown in Fig. 11. They

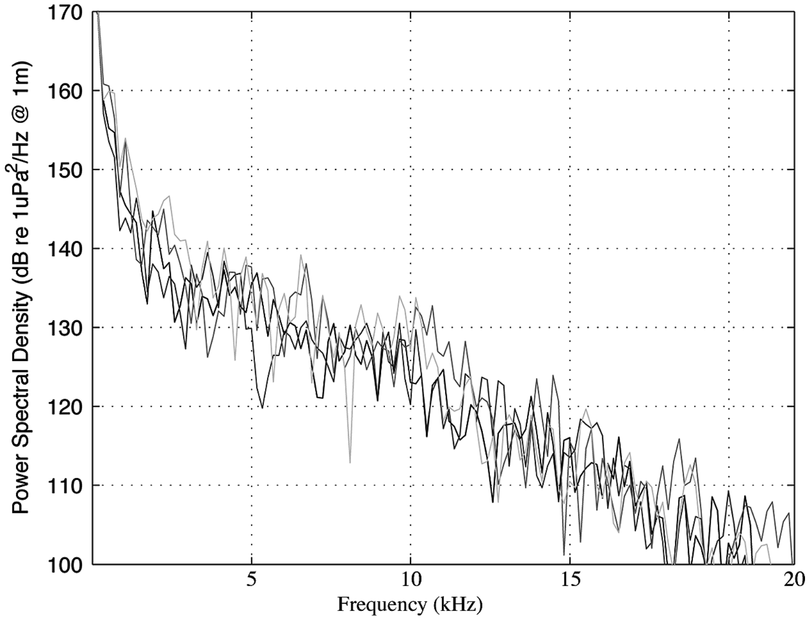

Fig. 9. High-frequency spectra for airgun 2–3 (195 in^3) over four separate shots.

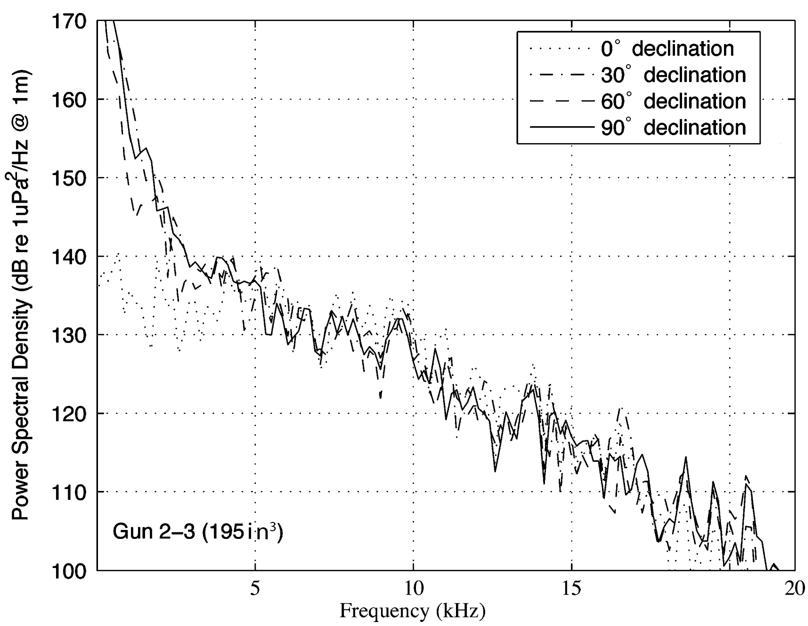

Fig. 10. Simulated airgun directionality for airgun 2–3 as a function of declination from the horizontal.

show that declination is predicted to have a very substantial impact on the output of the array at lower frequencies; 30–40 dB at <500 Hz from directly downwards to horizontally. These differences diminish as the frequency increases.

It is also clear that there are substantial variations with azimuthal angle, arising from the detailed coherent interference of many sources as the geometry changes. These can apparently introduce a variability of $+/-10$ dB. These predictions suggest that , based solely on amplitude, marine mammals may not be able to know whether they are swimming towards or away from a seismic array, because geometrical variations may give rise to $+/-10$ dB in received level purely as a result of changing azimuthal angle to the array without changing range.

VI. Marine Mammal Vocalization Denoising

The marine mammal vocalization recordings consist of various types, recorded on the two hydrophones of SPACMS. The recordings have significant transient noise caused by the survey vessel thrusters, and some unwanted tonal content. By cross correlating the two channels, the difference in arrival times of the marine mammal vocalization can be estimated to obtain a bearing. By time shifting by the difference in arrival time, and summing the two channels, one can increase the signal-to-noise ratio (SNR).

The data were denoised by a two-stage wavelet decomposition process, using the acoustical signal characterization toolbox (ASC), developed by the Acoustic Research Laboratory (ARL)

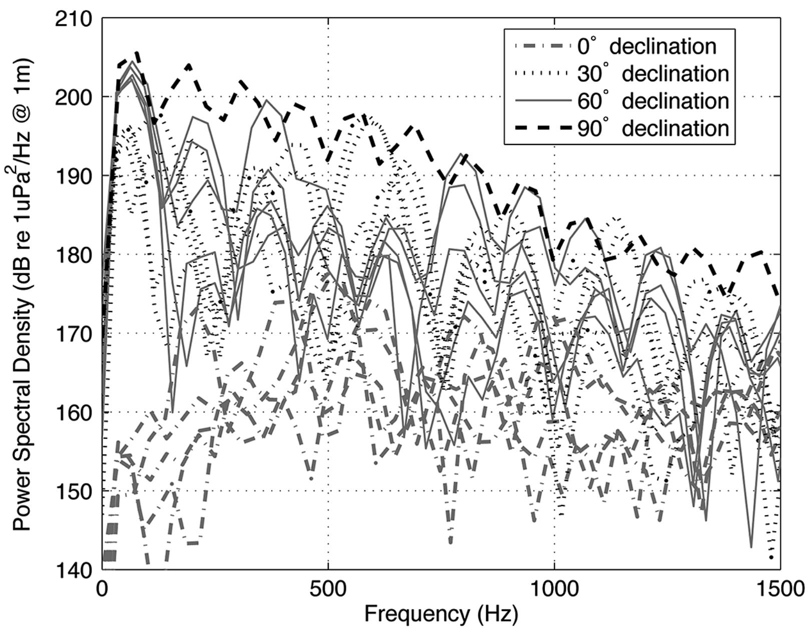

Fig. 11. Predicted declination and azimuthal variations in power spectral density of a seismic array above 150 Hz.

in the Tropical Marine Science Institute (TMSI) at the National University of Singapore (NUS) [6]. We present this approach since it is not computationally intensive and could be applied in real time as an aid to observers and operators.

By using the appropriate multiresolution transform, the ASC toolbox can be used to separate a time signal into the following components, extracting one at each stage of the process:

- tonals: long duration, frequency-localized signal;
- transients: broadband, time-localized signal;
- time-frequency transients;
- spectrally smooth noise.

Each denoising stage has a similar approach as follows:

- signal decomposition on an appropriate basis;
- signal detection;
- signal extraction and reconstruction.

Since the recordings exhibit mostly transient and tonal noise, only these extraction stages were used on the data.

A. Tonal Detection and Extraction

By definition, a tonal is a temporally long, frequency-localized signal. To achieve the best representation in the frequency domain, the most appropriate transform is a cosine-packet transform (CPT) [7].

Essentially, the coefficients of the transform are given by

$$\alpha_{j,k} = \langle s(n), \psi_{j,k} \rangle. \tag{11}$$

where $s(n)$ is the time series of the signal and $\psi_{j,k}$ is the cosine packet scaled by (j) and translated by (k) for $j = 0, 1, \ldots$ and $k = 0, \ldots, 2^j - 1$.

The cosine packet is a cosine wave multiplied by a smooth envelope function, so is well localized in both time and space, initially scaled to be the same length as the signal. At the zero level, $j = 0$, the transform is equivalent to a cosine transform of the whole signal. On the first level, $j = 1$ and $k = 0$, the cosine packet is scaled to half the length of the signal and the transform is equivalent to a cosine transform on the first half of the signal resulting in $\alpha_{1,0}$. When $j = 1$ and $k = 1$, the cosine packet is scaled to half the length of the signal and translated such that the transform is equivalent to a cosine transform on the second half of the signal resulting in $\alpha_{1,1}$. This process can be continued down to a finite number of levels; each level of the decomposition contains the complete representation of the signal, but split over different time windows; hence, it is a redundant basis representation of the original time signal. For this application, we are only concerned with the first-level coefficients. Further details of cosine-packet decompositions and wavelets-packet decompositions can be found in works in [7] and [8].

Tonal detection can be achieved by comparing the Shannon entropy function [9] of the coefficients at the first decomposition level to those for the zero level. The Shannon entropy is given by

$$P(\alpha_{j,k}) = -\sum \alpha_{j,k}{}^2 \log(\alpha_{j,k}{}^2). \tag{12}$$

If tonals are present, they will be present in both $\alpha_{1,0}$ and $\alpha_{1,1}$, since by definition they should be in the first and second half of the signal. Hence, the sum of the entropies of $\alpha_{1,0}$ and $\alpha_{1,1}$ should exceed the entropy of $\alpha_{0,0}$ since the first level essentially contains "more information" than the zero level.

To accurately locate tonal components, a dot-product is performed between the two level 1 coefficient vectors, and the square root taken to preserve the amplitude of the common frequency components.

A threshold was then applied to the correlation result to detect matching components between the two basis vectors at level 1. To remain adaptively objective, the Donoho–Johnstone estimator (DJE) [10] was used to estimate the threshold level. This requires the standard deviation of the assumed noise to be

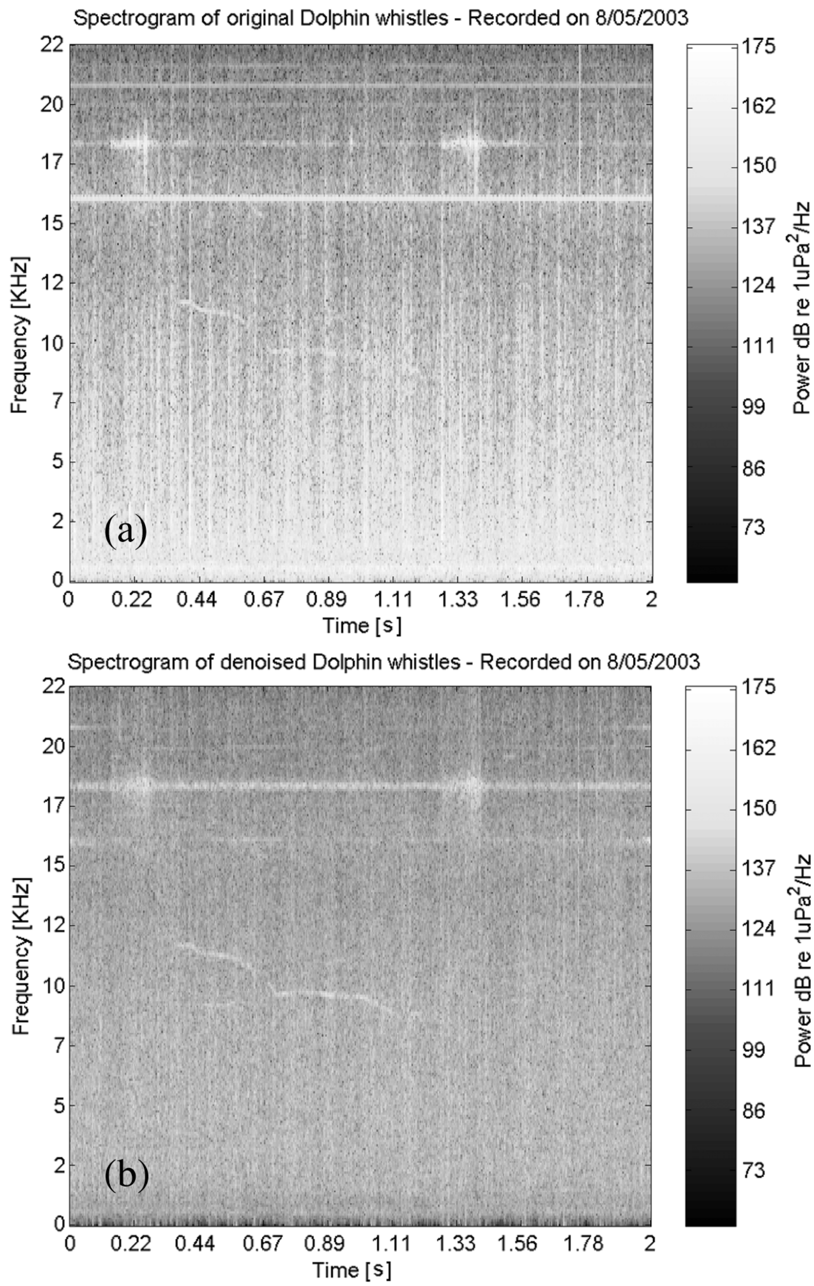

Fig. 12. (a) Original and (b) denoised spectrograms of a dolphin whistle.

known, and estimates can be sought from the zero level of the cosine-packet coefficients. The threshold t is given by

$$t = \sqrt{2 \ln N} \frac{M[\alpha_{0,0}]}{0.6745}. \tag{13}$$

where $M[\cdot]$ denotes the median and N is the length of the signal.

The threshold allows splitting of the signal into T (which contains the tonals), and a remainder R

$$\begin{aligned} T_{1,i} &= \left\langle c_{1,i}, \sqrt{\langle \alpha_{1,0}, \alpha_{1,1} \rangle} > t \right\rangle \Big|_{i=1,2} \\ R_{1,i} &= \left\langle c_{1,i}, \sqrt{\langle \alpha_{1,0}, \alpha_{1,1} \rangle} \leq t \right\rangle \Big|_{i=1,2}. \end{aligned} \tag{14}$$

T and R may then be reconstructed (since cosine-packet decomposition is orthogonal) to give the time series $T(n)$ and $R(n)$.

B. Transient Detection and Extraction

The same principle is applied to detect transients, the only difference being that orthogonal or biorthogonal wavelet-packet decomposition is used instead of cosine-packet decomposition.

Wavelets are compactly supported over a time interval but are generally not compactly supported in frequency. Wavelet-packet decomposition is the time/frequency dual of cosine-packet decomposition. Translation of the wavelet function corresponds to a shift in frequency (rather than time). Scaling of the wavelet function corresponds to a decrease in time resolution (rather than frequency).

Daubechies real biorthogonal most selective (DRBMS) wavelets were used with length $M = 22$, to obtain a good compromise between computation-time and efficiency.

The wavelet-packet decomposition (to level 1) of the signal is calculated. A true time transient that is broadband in frequency should show up in both halves of the level 1 coefficients. The entropy test is used to check for the presence of transients and the threshold is set using the same scheme as in the tonal extraction; the coefficients are split and reconstructed to yield the transient time series and the remaining times series.

C. Example Denoising Results

Denoising is shown for a dolphin whistle recorded on May 8, 2003, with the original and denoised spectrograms shown in Fig. 12. The recording was made shortly before dawn when the seismic source was "off" in a water depth of 550 m and at a range of 300 m. Fig. 12(a) shows strong noise tonals and broadband low-frequency noise that are largely removed in the denoised spectrogram of Fig. 12(b). As a result, the frequency-modulated whistle in the center of the frequency range is much clearer in the denoised spectrogram. Other examples exhibit comparable performance.

While it would have been desirable to obtain good recordings of the northern bottlenose whale, only weak records of their clicks were available. These were sufficient to identify the species, but not of sufficient quality to warrant further study.

VII. Conclusion

The marine mammal observation data collected during EnCana's Stonehouse seismic survey shows no evidence of significant individual impact on marine mammals, including northern bottlenose whales. The data analysis indicates statistically significant responses from marine mammals to seismic activity (i.e., to stay outside a close approach circle, to be observed in larger groups, and to reduce vocalizations but not to move out of detection range). It should be noted however, that the results from this data gathering effort may be affected by potential sources of bias (such as the combination of data from toothed and baleen whales).

In addition, the SPACMS has proved itself a valuable marine mammal observation tool that can usefully complement visual observations. SPACMS produced detections that were uncorrelated with visual observations, hence providing new information unavailable to visual observers. The data from SPACMS has also been used to infer high-frequency behavior of the seismic source elements and likely far-field array effects, including estimated received levels at various angles in azimuth and declination from the seismic arrays. This analysis confirmed that most of the seismic energy was concentrated at lower frequencies (<500 Hz).

Finally, we have presented an example spectrogram of a marine mammal recording and suggested a denoising toolbox that could be used to improve detection of marine mammal vocalizations.

Acknowledgment

The authors would like to thank the teams who made these observations possible, at EnCana Corporation and Seamap Pte Ltd., and the support of EnCana Management to seeing the observations worked up and published.

References

[1] Committee on the Status of Endangered Wildlife in Canada (COSEWIC), "COSEWIC assessment and update status report on the northern bottlenose whale *Hyperoodon ampullatus* (Scotian Shelf population) in Canada" Ottawa, ON, Canada, 2002.

[2] National Marine Fisheries Service, "Bahamas marine mammal stranding event of 15–16 March 2000. Joint interim report by National Marine Fisheries Service and Department of the Navy" Dec. 2001.

[3] J. C. Goold and P. J. Fish, "Broadband spectra of seismic survey air-gun emissions with reference to dolphin auditory thresholds," *J. Acoust. Soc. Amer.*, vol. 103, pp. 2177–2184, 1998.

[4] R. J. Urick, *Principles of Underwater Sound*, 3rd ed. New York: McGraw-Hill, 1983, p. 131.

[5] W. S. Cleaveland, "Locally weighted regression: An approach to regression analysis by local fitting," *J. Amer. Statist. Assoc.*, vol. 83, pp. 596–610, 1988.

[6] E. Delory and J. R. Potter, "Signal processing aspect of signal detection masking and noise suppression," in *Proc. Acoust. Vibration Asia'98*, Singapore, Nov. 1998, pp. 291–300.

[7] S. Mallat, *A Wavelet Tour of Signal Processing*. New York: Academic, 1998.

[8] M. V. Wickerhauser, "Comparison of picture compression methods: Wavelet, wavelet packet and local cosine transform coding," in *Wavelets: Theory, Algorithms and Applications*, C.K. Chui, L. Montefusco, and L. Puccio, Eds. New York: Academic, 1994, pp. 585–621.

[9] M. Bouvet, *Traitements des Signaux Pour Les Systèmes Sonar*. New York: Masson, 1992.

[10] D. L. Donoho and M. J. Iain, "Adapting to Unknown Smoothness via Wavelet Shrinkage," *J. Amer. Statist. Assoc.*, vol. 90, no. 432, pp. 1200–1224, Dec. 1995.

John R. Potter (M'95–SM'02) received a joint honors degree in mathematics and physics from Bristol University, Bristol, U.K., in 1979 and the Ph.D. degree in glaciology and oceanography from the Council of National Academic Awards in association with the University of Cambridge, Cambridge, U.K., in 1985.

He worked for the British Antarctic Survey from 1980 to 1985, spending four research summers in the Antarctic. From 1986 to 1991, he was a Senior Scientist for NATO SACLANT Undersea Research Centre (SACLANTCEN), La Spezia, Italy, working on high-frequency acoustics, followed by a term as a Research Project Scientist at Scripps Institution of Oceanography, San Diego, CA, from 1991 to 1995. In 1996, he founded and remains a Head of the Acoustic Research Laboratory (ARL) and is currently an Associate Director of the Tropical Marine Science Institute in the National University of Singapore (NUS), Singapore.

Dr. Potter is a member of the Acoustical Society of America, an International Fellow of the Explorer's Club, a Master Scuba Diver Trainer with the Professional Association of Dive Instructors, Chairman of the IEEE Oceanic Engineering Society in Singapore and Co-Chair of OCEANS Asia Pacific 2006 Conference. He was awarded the Polar Medal by Queen Elizabeth II, received the "Best Paper" Award in 1996 for an article in *Scientific American*, and was the Principal Investigator for the team that won the Defence Technology Prize in Singapore, in 2004.

Marielle Thillet received the multidisciplinary engineering degree from the Ecole Supérieure d'Ingénieurs de Marseille, Marseille Cedex, France, in 1999, the M.Sc. degree in marine technology from Cranfield University, Cranfield, U.K., in 2000, the certificate in environmental management from Dalhousie University, Halifax, NS, Canada, in 2004, and the professional engineer certification from the Province of Nova Scotia, Canada, in 2004.

She is currently working as an Environmental Advisor for EnCana Corporation, Halifax, NS, Canada, and is supervising all environmental activities for EnCana's Canadian East Coast operations.

Craig Douglas received the B.Sc. honors degree in computer systems engineering from the University of Kent, Canterbury, U.K., in 1987.

From 1988 to 2001, he worked for Schlumberger in a variety of roles including Research Vessels Technician, Chief Observer Onboard, Senior Project Engineer, and Department Technical Manager. In 2000, he began working with Seamap Pte. Ltd., Singapore, as a Vice President of Technology, where he remained until 2005. He is now an independent Oil Exploration Industry Consultant.

Mandar A. Chitre (M'04) received the B.Eng. and M.Eng. degrees in electrical engineering from the National University of Singapore (NUS), Singapore, in 1997 and 2000, respectively, the M.Sc. degree in bioinformatics from the Nanyang Technological University, Singapore, in 2004, and is currently working towards the Ph.D. degree via research in underwater acoustics communication at NUS.

From 1996 to 1998, he worked with the Acoustic Research Laboratory (ARL), National University of Singapore (NUS), Singapore. From 1998 to 2002, he headed the technology division of a South East Asian telecommunications software company. In 2003, he rejoined ARL, where he is currently the Deputy Head (Research).

Mr. Chitre is a Secretary for the IEEE Oceanic Engineering Society (Singapore Chapter). He is also the Chairman of the Student Poster Committee for the Oceans 2006 Asia-Pacific–Singapore Conference.

Zbigniew Doborzynski received the engineering degree in mining engineering and applied geophysics and the M.S. degree in applied geophysics from McGill University, Montreal, QC, Canada, in 1971 and 1974, respectively.

He joined Imperial Oil Ltd. as a Minerals Geophysicist in 1973 and was responsible for acquisition, processing, and interpretation of geophysical data mainly in eastern Canada. From 1979 to 1989, as a Senior Minerals Geophysicist, he coordinated geophysical activities across Canada for ESSO Minerals Canada. In 1989, he transferred to ESSO Resources Canada to acquire geophysical data for oil and gas exploration in the McKenzie Delta, Western Canadian Basin, and offshore Nova Scotia. In 2001, he joined PanCanadian Petroleum Ltd., later renamed EnCana Corporation, Calgary, AB, Canada, as a Manager of Marine Acquisition and is responsible for all aspects of marine geophysical and geotechnical data acquisition worldwide.

Mr. Doborzynski is a registered Professional Engineer of Ontario and member of both the Society of Exploration Geophysicists (SEG) and the Canadian Society of Exploration Geophysicists (CSEG).

Paul J. Seekings was born in England in 1974. He received the B.Eng. (honors) degree in electronics, music and media and the Ph.D. degree in multidimensional control systems (applied mathematics), both from Leeds Metropolitan University, Leeds, U.K., in 1996 and 2000, respectively.

He is currently a Research Fellow at the Acoustic Research Laboratory (ARL), National University of Singapore (NUS), Singapore. His current research interests are array signal processing, denoising and signal separation, and advanced sensing techniques.